Figure of Merit of All-Dielectric Waveguide Structures for Absorption Overtone Spectroscopy

Aviad Katiyi and Alina Karabchevsky

Abstract—The figure of merit is proposed for all-dielectric waveguides for absorption overtone spectroscopy as the measure of probing efficiency of molecular overtones. It is defined as the power in the evanescent tail over the total power carried by the guided mode. The figure of merit was calculated for the proposed waveguide structures and then compared. We address each waveguide structure in probing overtones. We show that the figure of merit can be substantially increased due to the downscaling of the physical dimensions of the waveguide and microfiber. Such a configuration enables integration possibilities for ultrasensitive devices harnessing evanescent excitation of molecular overtones on miniature and portable chips.

Index Terms—Integrated optics, optical design and fabrication, optical devices, spectroscopy, thin films.

I. INTRODUCTION

SINCE the development of the laser in the early 1960s, the guided wave optics has attracted much of interest. Guided wave optics has enabled the discovery of novel optical phenomena, such as the diffusive propagation of light in a waveguide [1]. It facilitates a wide range of technological advancements (e.g., miniaturization, affordability and mobility [2]) and overcomes scientific challenges [3], such as guiding at the Dirac frequency beyond photonic bandgaps [4]. The key element in guided wave optics is the waveguide [3]. Experimental study shown, that a waveguide can be efficiently utilized to detect the molecular overtones of anilines and to study their molecular dynamics [1]. Aniline and its derivatives are widely used in the dye industry and in pharmaceuticals. The primary aniline molecule (Fig. 1(a)), which was probably first used during the 18th century [5], has $n = 14$ atoms and $3n - 6 = 36$ normal modes of vibration. Since the overtones and combination modes of aniline are infrared-active, they can be studied by near-infrared spectroscopy; however, since overtone transitions have weaker intensities than fundamental transitions, they are challenging to detect and it is, therefore, essential to find a structure for efficient overtone spectroscopy. Here we theoretically study passive guided-wave optical components for an efficient overtone spectroscopy. We summarize our results to study the first overtones of amines having a transition $v = 0 \rightarrow v = 2$, observed
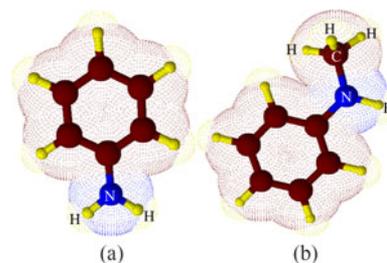
Fig. 1. Molecular structures of (a) the primary amine aniline $C_6H_5NH_2$ and (b) the secondary amine N-methylaniline $C_6H_5NH(CH_3)$.

with guided-wave optics at telecommunication wavelengths of 1.5 μm [1], [6], [7].

Although various "figure of merit" FoM of waveguides including non-linear Kerr plasmonic waveguides have been proposed for sensing and waveguiding applications, emission enhancement, and nanolasers [8]–[13], the FoM for overtones absorption phenomenon is not well established. First, detecting overtones with waveguides, as an alternative approach to mid-infrared spectroscopy, requires probing a quality measure, or a (FoM). Such a FoM for detecting molecular overtones with waveguide architectures has not been proposed previously, and it would be useful for comparing different waveguide architectures, material choices, fabrication considerations, and operating wavelengths.

In this study, FoM is proposed for straight waveguides, tapered waveguides, and microfibers; then, it used to compare and assess most common waveguide architectures and conventional microfibers. Section II presents the numerical methodology used in this study and the rationale behind using monomode waveguide architectures for overtone spectroscopy. Section III defines the FoM and provides calculated results for most common waveguide architectures. Section IV details the calculated dispersion of the probe molecule and discusses the strategy for improving the FoM. Concluding remarks are given in Section V.

II. NUMERICAL MODELING

A. The Probe Molecule

In their pioneering work on the overtone spectroscopy of anilines, Karabchevsky and Kavokin [1] detected a well-defined amine (N-H) band in the aniline derivative N-methylanilne (Fig. 1(b)) in optically weak, diffused waveguides. This effect was explained in terms of a switch from a ballistic to a diffusive propagation of light by strong scatters (the molecules)
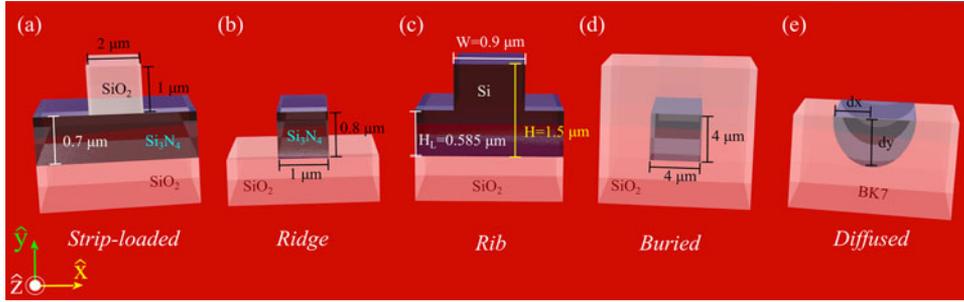
Fig. 2. Rendered images of common laterally confined passive waveguide structures: (a) a strip-loaded waveguide made of nitride on a silica substrate covered by silica, (b) a ridge waveguide made of nitride on a silica substrate, (c) a rib waveguide made of silicon on a silica substrate, (d) a waveguide buried in silica glass, and (e) a diffused waveguide in borosilicate glass. The dimensions of the structures considered in this study are labeled.

adsorbed on the surface of the device. Here, we explore passive waveguides that allow efficient overtone spectroscopy in the near-infrared spectrum. The structures that we study are shown in Fig. 2 and include a strip-loaded waveguide (Fig. 2(a)), a ridge waveguide (Fig. 2(b)), a rib waveguide (Fig. 2(c)), a buried waveguide (Fig. 2(d)), and a diffused waveguide (Fig. 2(e)).

Somewhat analogous to an electrical current that is guided by a metallic strip (a key element in an electrical integrated circuit), the photonic waveguide enables photons to flow in a controlled manner. A passive photonic waveguide is a key element in a photonic integrated circuitry, and was initially implemented for telecommunication applications [3]. The passive photonic waveguides enable the spatial distribution of optical energy in one dimension, as in a slab waveguide, or in two dimensions, as in laterally confined waveguides. Here, we propose and analyze a scheme for the extent of the fundamental optical mode, overlapping with the organic mixture, for an efficient excitation of amine overtones in the near-infrared spectrum. We address each waveguide structure shown in Fig. 2 in probing these overtones. We calculate the zero-order optical mode - an electric or a magnetic field (within electrostatic approximation), which is the solution of the wave equation for linearly polarized light [14]. The shape of the mode varies with waveguide geometries and materials.

When multiple modes propagate through the waveguide, the energy of the incident wave is non-uniformly divided between the modes. Higher-order modes propagate at bigger inclination angles, given by electromagnetic wave analysis [14], and exhibit scattering losses due to surface defects that are induced during the fabrication routines. The variety of modes also raises the modal dispersion, which decreases the signal-to-noise ratio. Hence, we consider monomode waveguides in our numerical model.

Numerical modeling has been performed here by using a finite-element method (FEM) implemented in COMSOL Multiphysics 5.2. We define the waveguide dimensions based on the refractive index contrast Δ for a single-mode operation, such that - $\Delta = (n_1 - n_2)/(n_1)$, where n_1 and n_2 are the indices of the guiding layer and the superstrate (or substrate), respectively.

B. Slab Waveguide

The slab waveguide is modeled as a guiding layer, which is located above the substrate layer. The height required to support
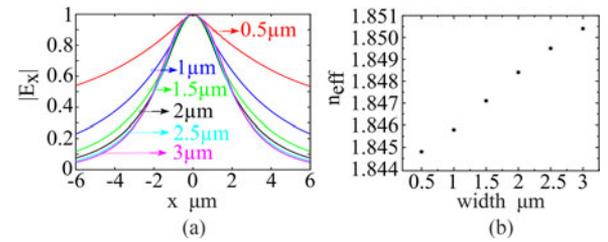

Fig. 3. Quasi-TE polarization. $|E_x(x,y)|$ modes normalized to the maximum amplitude while varying the width of the strip in strip-loaded waveguides. The indicated values represent the strip width. (a) The cross-section profiles ; (b) the change in the effective mode index of the waveguide width as function of strip width.

only the fundamental mode is [15]: $h < \lambda_0/[2(n_1^2 - n_2^2)^{1/2}]$ where λ_0 is the wavelength in a vacuum.

C. Strip-Loaded Waveguide

Fig. 2(a) shows a strip-loaded waveguide. To confine the light in the x-plane, a metal or dielectric strip is placed on top of the slab waveguide. Increasing the strip width enhances the confinement. Fig. 3 shows the evolution of the normalized electric field amplitude at quasi-TE polarization with strip width w. The field confines laterally with increasing strip width, leading to an increase in the effective mode index of the structure (Fig. 3(b)). The maximal strip width can be obtained when the effective mode index reaches the index of the guiding layer (here 1.99).

D. Ridge Waveguide

In the ridge waveguide geometry (Fig. 2(b)) the guiding layer is made of a strip. We consider a Si_3N_4 ridge waveguide, which is CMOS-compatible. The dispersion of the Si_3N_4 depends on the ratio between silicon to nitrogen [16]. The surrounding medium has a lower refractive index than that of the guiding layer, resulting in a high confinement in the guiding layer of this structure. The substrate is usually silica (SiO_2), grown on a Si wafer.

E. Rib Waveguide

Although the rib waveguide (Fig. 2(c)) is very similar in appearance to the strip-loaded waveguide, the strip is made of the same material as that of the guiding layer. Consequently, the guiding layer has two different height areas. By adjusting

the height and width of the strip, one can make a rib wave-guide, supporting a single mode, quite big. This will lead to the compatibility with optical fibers and facilitate the coupling in and out the waveguide. Assuming the rib structure equation for a monomode operation [17], [18] yields:

$$W/H = 0.3 + r/(1 - r^2)^{1/2} \rightarrow r \geq 0.3 \qquad (1)$$

$$H_L = rH \qquad (2)$$

With strip width W, height H, height of the Si slab film H_L. The strip dictates the lateral confinement of the fundamental mode. The higher modes are cut off. Since the fundamental mode has less contact with edges due to its guiding layer shape, a rib waveguide exhibits lower scattering loss. Rib waveguide, operating in the single mode regime, is of bigger dimensions compared to the ridge waveguide made of the same materials. This makes the coupling easier - the main advantage of this structure.

F. Buried Channel Waveguide

The buried channel waveguide (Fig. 2(d)) has a symmetrical geometry. Similarly to the fiber, its guiding layer is surrounded by a dielectric material with a low refractive index. A barried waveguide is fabricated using helium plasma reactor to dissect silane and oxygen and deposit the silicon dioxide on the wafer. Here, fluorine is used to dope a substrate in order to fabricate a buried channel waveguide in the silica [19], [20]. Another possibility is to fuse the silica with a megaelectronvolt beam of protons focused down to a few micrometers [21]. The most common configuration of the buried waveguide is fiber, as its flexibility, low propagation losses (0.5 dB/km for a 1.55 μm single mode fiber SMF), and low price makes it adequate for transferring communication and data over long distances. Although it results in an optically weak waveguide, this structure is advantageous due to the affordability of silica and the simplicity of fabrication.

G. Diffused Channel Waveguide

The substrate layer of a diffused-channel waveguide is made of materials such as soda lime glass, Pyrex, Corning 3-71, or borosilicate (BK7) [22], [23]. BK7 is the most common material used for the substrate due to its high concentration of Na, which can be easily exchanged with cations (such as K^+ and Ag^+) and high coupling efficiency with silica fibers. As the fabrication process involves ion-exchange [1], the refractive index varies non-linearly with the cross section of the substrate.

$$n(x, y) = n_s + \Delta n \cdot erfc(y/dy) \exp(-x^2/dx^2) \qquad (3)$$

With refractive index of substrate n_s, dx and dy are the penetration depths in x and y directions respectively, Δn is the maximal index change. The extraordinary performance of the diffused-channel waveguide as a near-infrared spectrophotometer was demonstrated in [1].

The mask opening defines the penetration depth and width of the ion-exchange, and the type of ions implanted inside the glass defines the optical properties of the core, Δn [24]. For instance,
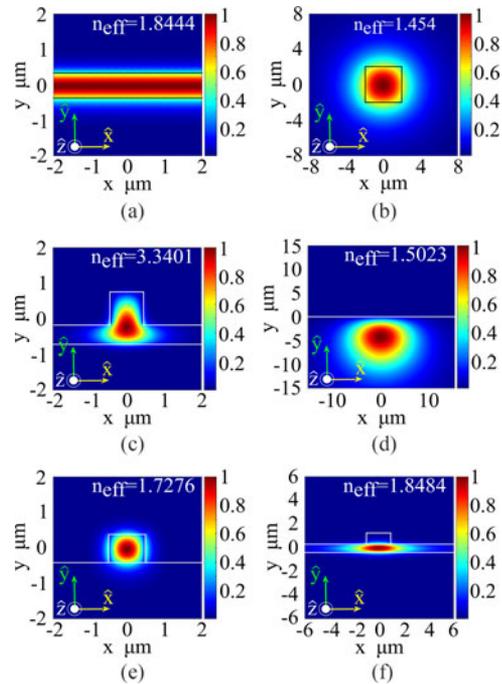

Fig. 4. Quasi-TE polarization. Colormaps of $|E_x(x, y)|$, normalized to the maximum amplitude in monomode waveguides: (a) planar, (b) buried, (c) rib, (d) diffused, (e) ridge, and (f) strip-loaded.

$\Delta n = 0.009$ for KNO_3 and $\Delta n = 0.028$ for $AgNO_3$. The main advantage of an ion-exchange waveguide is its low propagation losses, although its structure is an optically weak ($\Delta = 0.5\%$ in BK7, using KNO_3).

The simplest way of coupling light between waveguides is a butt-coupling. In butt-coupling the end surfaces of the two waveguides are facing each other at a junction. Naturally, at such a junction, might be a gap and misalignment between adjacent waveguides. These offsets are considered to affect significantly the coupling efficiency. In addition, if the waveguides are not identical in terms of materials and architecture the modal mismatch between the waveguides will affect the coupling efficiency.

As mentioned above, we consider here a single-mode waveguide for absorption overtone spectroscopy. We calculate the dimensions of a waveguide and the field distributions E_x and E_y for quasi-TE and quasi-TM polarization, respectively, by using FEM of COMSOL Multiphysics. Numerical models were created using the Wave Optics module of COMSOL Multiphysics 5.2. The mesh was set as extremely fine to obtain the accurate solution of the wave equation in studies waveguide structures with electric conductor boundary conditions. The calculation results are provided in Figs. 4 and 5. Fig. 4 shows the x component of the electric field amplitude for a quasi-TE mode, normalized to its maximal amplitude. Fig. 5 shows the y component of the electric field amplitude for a quasi-TM mode, normalized to the maximum. The planar waveguide (Fig. 4(a) and (b)) shows a higher field at the interface between the guiding layer and the superstrate in the TM mode. In buried channel waveguide, due to its low Δ, fraction of the energy which propagates outside the guiding layer regardless of the mode (Figs. 4(b) and 5(b)). The field
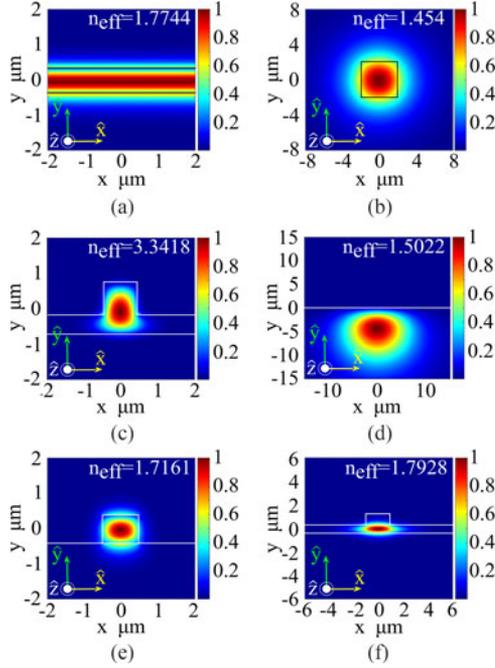
Fig. 5. Quasi-TM polarizaiton. Colormaps of $|E_y(x,y)|$, normalized to the maximum amplitude in monomode waveguides: (a) planar, (b) buried, (c) rib, (d) diffused, (e) ridge, and (f) strip-loaded.
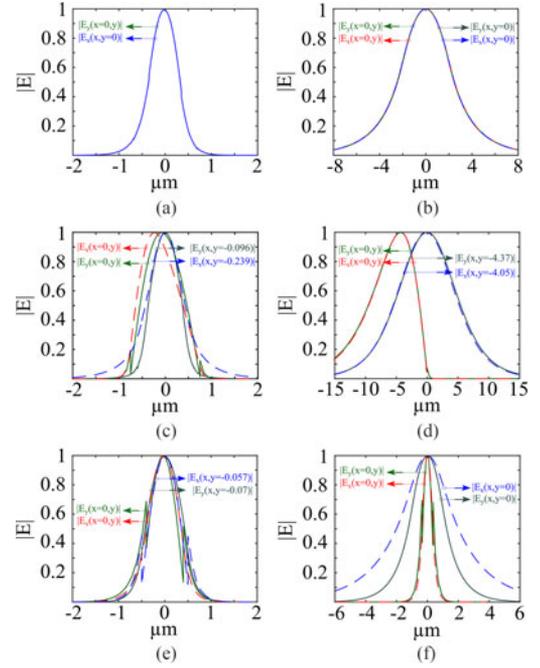

Fig. 6. Cross-section profiles of the normalized electric field amplitudes shown in Figs. 4 and 5: (a) planar, (b) buried, (c) rib, (d) diffused, (e) ridge, and (f) strip loaded.

is well-confined in the guiding layer of the rib waveguide [to a lesser extent in quasi-TE (Fig. 4(c)) and to a greater extent in quasi-TM (Fig. 5(c))] for both orthogonal polarizations and because the mode interacts less with the edges. The ridge waveguide (Figs. 4(c) and 5(c)) is less confined in the guiding layer than the rib waveguide. The strip in the strip-loaded waveguide enables mode confinement in the $\hat{x}$ direction. E_y demonstrates a higher confinement in the $\hat{x}$ direction and a higher evanescent field. Figs. 4(d) and 5(d) show the mode profiles of a diffused waveguide. A non-confined mode results from low Δ and from the diffusive nature of waveguide's fabrication. The modal distributions of ridge waveguides (Figs. 4(e) and 5(e)) show good confinement in the guiding layer and evanescent tails outside its physical dimension.

To gain a deeper understanding of the differences between the modal distributions in the different waveguide structures, we compare the cross section at the maximal value of the field in the $\hat{x}$ and in $\hat{y}$ directions.

Fig. 6 shows the cross-section profiles of the normalized electric field amplitudes. Fig. 6(a), (b), and (d) shows that the normalized electric field amplitude in quasi-TE and quasi-TM polarizations on planar buried and diffused waveguides, which have the same cross-section. Fig. 6(e) shows that the cross-section in a quasi-TE polarization, which is much wider than in the quasi-TM polarization.

III. FIGURE OF MERIT

To compare and assess the most common waveguide architectures used for absorption overtone spectroscopy, we define the FoM as the power carried by the evanescent tail over the total power carried by the mode, as can be seen in (4). We define the

TABLE I
FRACTION OF THE POWER PROPAGATING IN MONOMODE WAVEGUIDES IN AIR

Waveguide	quasi-TE		quasi-TM	
type	η_{core}	FoM	η_{core}	FoM
ridge	0.909714	0.036623	0.895611	0.041313
slab	0.912614	0.027938	0.899022	0.016637
rib	0.992363	0.003658	0.99354	0.005943
diffused	0.999851	0.000127	0.999947	5.18E-05
strip	0.904182	0.012921	0.886581	0.004783

fraction of power in the core of the waveguide structure shown in (5):

$$FoM = \eta_{\mathrm{evan}} = P_{\mathrm{evan}}/P_{\mathrm{total}}$$

$$= \int_{\mathrm{sup}} S dA \bigg/ \int_{-\infty}^{\infty} S dA \qquad (4)$$

$$\eta_{\mathrm{core}} = P_{\mathrm{core}}/P_{\mathrm{total}} = \int_{\mathrm{core}} S dA \bigg/ \int_{-\infty}^{\infty} S dA \qquad (5)$$

Note: Since absorption is caused due to complex refractive index of the molecule, electric E and magnetic H fields in a waveguide evolve as complex, therefore the real part of the Poynting vector S, which is the propagating power per unit area, A, has to be considered: $S = 1/2\mathcal{R}(E \times H^*)$ [25].

Table I summarizes the calculated data for waveguides embedded in air. It indicates the fraction of the power propagating in a waveguide core and beyond its physical dimensions for quasi TE and quasi TM polarizations.

The FoM calculations show that, of all examined waveguide architectures, the ridge waveguide configuration has a maximal interaction with the superstrate which is more than 3.5%.

Evanescent excitation has its advantages in sensing [26]–[28]. Since we aim at utilizing evanescent fields for spectroscopic ap-
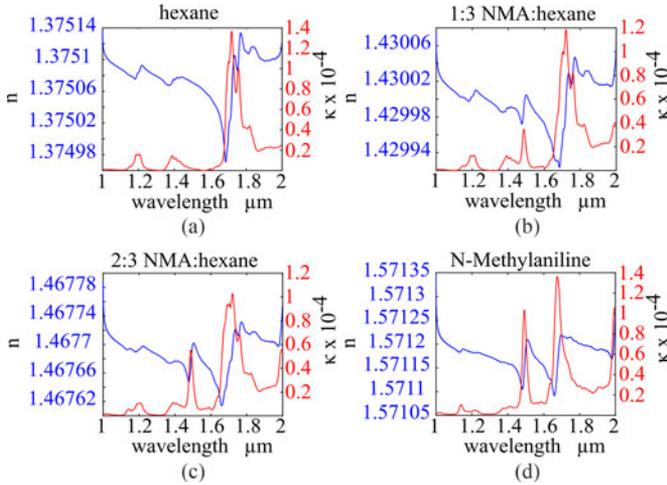
Fig. 7. Dispersion of (a) hexane, (b) mixture ratio 1:3 of N-Methylaniline to hexane, (c) mixture ratio 2:3 of N-Methylaniline to hexane, and (d) pure NMA calculated by using the KK relation.

TABLE II
FRACTION OF THE POWER PROPAGATING IN MONOMODE WAVEGUIDE EMBEDDED IN MIXTURE RATIO 1:3 OF N-METHYLANILINE TO HEXANE

| Waveguide | quasi-TE | | quasi-TM | |
type	η_{core}	FoM	η_{core}	FoM
ridge	0.868213	0.0868	0.858926	0.094387
slab	0.896623	0.050775	0.88289	0.056531
rib	0.991583	0.004672	0.992465	0.006981
diffused	0.99819	0.001783	0.998398	0.001603

Fig. 8. Tapered waveguide structures: (a) tapered ridge waveguide, (b) micro-fiber.

plications, and since the extent of the field distribution strongly dependent on the waveguide dimensions, it is necessary to evaluate the suitable dimensions for particular applications.

Thus, we consider bulk molecules in our model and evaluate their optical properties with a complex refractive index $n = n + j\kappa$. We evaluate the extinction coefficient κ from the measured absorption by using a cuvette with a 1 mm path length (measured with Jasco VIS-NIR spectrophotometer) and calculate the index n by using the Kramers-Kroning (KK) relation [29] implemented in Matlab with the Hilbert transform:

$$n(\omega) - 1 = 2/\pi \cdot \mathcal{P} \int_0^\infty \omega' \kappa(\omega') / (\omega'^2 - \omega^2) \, d\omega' \quad (6)$$

Fig. 7 shows the dispersion of hexane (Fig. 7(a)) and its mixtures with the N-methylaniline (NMA) molecule. Fig. 7(b) shows mixture ratio 1:3 of N-Methylaniline to hexane, Fig. 7(c) shows mixture ratio 2:3 of N-Methylaniline to hexane, and Fig. 7(d) shows the dispersion of the pure NMA molecule.

IV. PROBING AN OVERTONE WITH WAVEGUIDES

Evanescent sensing [26], [28] is a widely used technique utilizing sub-diffraction limit gratings [30]–[33], sculptured thin films [34], [35] and nanoantennas [36]. We analyze the power in the evanescent field, as shown in (4), and in the core of the waveguides [as shown in (5)] while considering molecular mixtures (Fig. 7). We use the amine-based molecule NMA as a probe molecule to demonstrate the concept of probing molecular overtones with guided-wave optics in the near-infrared spectrum. We model the waveguides embedded in index of refraction related to the mixture ratio 1:3 of N-Methylaniline to hexane which is: $n(\lambda = 1.496\,\mu\text{m}) = 1.4299855 + j2.66917 \times 10^{-6}$. Mixture ratio 1:3 of N-Methylaniline to hexane was chosen to support the monomode propagation in a silica fiber.

Table II summarizes η_{evan} and η_{core} for waveguides embedded in the molecular mixture.

The FoM calculations in Table II show that the maximal power that can be carried by the evanescent field is obtained

with a ridge waveguide, and $FoM = 9.4\%$ for TM polarized light. However, for an efficient probing of the molecular layer, much more than 10% of the power in the evanescent field is required. Therefore, the waveguide design can be further optimized to obtain a higher FoM, which will increase the intensity and penetration depth of the evanescent field, resulting in a strong interaction with the surrounding medium. This interaction between the molecules and the evanescent field, or strictly speaking the figure of merit (FoM) can be defined as the fraction of the power in the evanescent tail over the total power carried by the mode. The implementation of such a probing can be realized either by using a high index contrast waveguide or by tapering a weak waveguide. Chemical surface preparation of the weak waveguide's is also possible for the probing of molecular overtones as was shown in [1]. In addition, to enhance the probing efficiency of the weak waveguide, one can utilize the diffusive regime phenomenon, as demonstrated in [1]. Tapering the guiding layer is an elegant approach to increase the FoM and strengthen the interaction between the evanescent field and the molecular medium.

A. Optimization of Device Geometry for an Efficient Field-Molecule Interaction

As was indicated in the previous section, we aim at tapering the waveguide such that the evanescent field gets increased resulting in improved FoM. Therefore, we propose the taper geometry shown in Fig. 8. Light from a straight monomode waveguide illuminates the tapered region Fig. 8 and is coupled back into the straight monomode waveguide for an efficient collection of the signal. We design the structure in such a way that the transition region is adiabatic to eliminate any energy transfer between modes and to lower scattering losses [37].

To compare between the waveguide structures, we minimize the guiding layer while still considering the practical fabrication limitations for obtaining the single mode performance. This comparative study is aimed to provide a systematic comparison
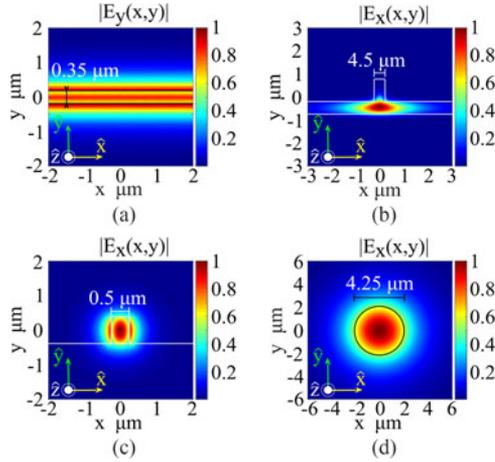
Fig. 9. Normalized electric field amplitude colormaps for waveguides embedded in the mixture ratio 1:3 of N-Methylaniline to hexane: (a) slab waveguide, (b) rib waveguide, (c) silicon nitride ridge waveguide on silica, and (d) silica microfiber.

TABLE III
FRACTION OF THE POWER CARRIED BY THE MODES OF TAPERED WAVEGUIDES EMBEDDED IN MOLECULAR MIXTURE (FIGS. 8 AND 9)

Waveguide type	η_{core}	FoM
ridge	0.598454	0.323221
slab	0.883412	0.056531
rib	0.978077	0.011161
fiber	0.67076	0.329247

between different waveguide architectures by minimizing the physical dimensions of the structures with the same rate to obtain a higher interaction of molecules with the evanescent field. Rib and ridge structures can become thinner only in the x-plane. Thinning in the y-plane can be accomplished only by changing the height off the guiding layer in a steps-like manner, resulting in high losses. Rather than the buried waveguide, we consider here a cylindrical fiber geometry. The core of a single-mode SMF1550 fiber is 9.5 μm, and, therfore, the taper should be 4.25 μm. A strip waveguide is less favorable, because the strip is basically a spacer that separates the core and molecular mixture. Naturally, a slab waveguide has no lateral confinement and becomes thinner only in the y-plane, with no transition region. In principle, it is possible to obtain a gradual thinning of the height in a step-like manner by using multiple masks. This procedure, however is not recommended due to high losses.

Fig. 9 shows the influence of a waveguide embedded in mixture ratio 1:3 of N-Methylaniline to hexane on the field distribution. Fig. 9(a)–(d) shows the calculated normalized electric field amplitudes of a slab, a rib, and a ridge waveguides, and of a microfiber, accordingly. Thinning the physical dimensions of the structures leads to increased evanescent field amplitudes in the superstrate.

In addition, we systematically calculated a FoM for each of the tapered waveguide configurations. These results are summarized in Table III, which compares between power fraction in the core of the waveguide architectures and their FoMs. The thinning of the structure can be seen to increase the FoM, as
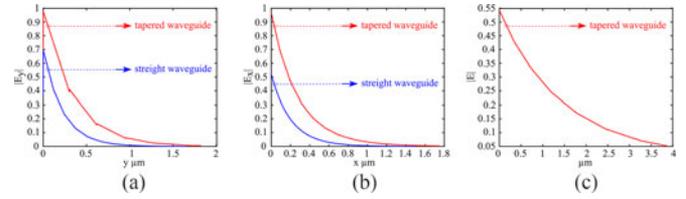

Fig. 10. Cross-section profiles of normalized electric field amplitudes of the evanescent field shown in Fig. 9 compared to cross-section profiles of normalized electric field amplitudes in monomode waveguides embedded in the mixture. (a) Slab waveguide, (b) Si_3N_4 ridge waveguide on silica, and (c) silica microfiber.
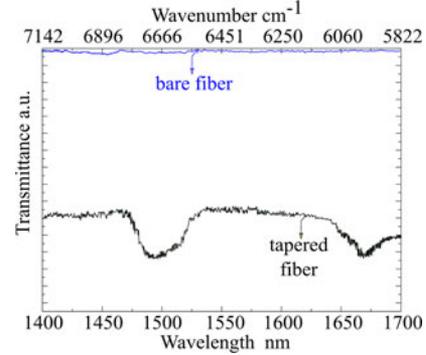

Fig. 11. Measured transmittance spectra on tapered fiber compared to a bare fiber.

compared with the values summarized in Table II. The ridge waveguide and the fiber show the highest FoM values, which is more than 30%.

Fig. 10(a)–(c) shows the evanescent fields extracted from the modes shown in Fig. 9(a), (c), and (d), respectively. These profiles are compared to the evanescent fields in monomode waveguides embedded in the molecular mixture. The amplitude of evanescent fields increases due to the minimizing of the guiding layer. However, according to Table III, the FoM of the slab waveguide is too small ($\sim$0.056) for absorption overtone spectroscopy and, therefore, the tapered slab architecture is less favorable for sensing applications.

V. PROOF-OF-CONCEPT EXPERIMENT

For the proof of concept experiment, we fabricated the tapered fibers by tapering a conventional SMF1550 fiber based on the modified flame brushing technique. The microheater was used to heat the fiber locally toward its softening point, then the fiber was pulled apart using micro-stages to minimize its diameter. We prepared the surface of the fiber to allow for molecular adsorption. During the spectroscopic measurement we dripped the molecular mixture ratio 1:3 of N-Methylaniline to hexane. Fig. 11 shows the experimental results of the transmittance with well-defined overtone resonances detected on a tapered fiber. As expected, on the bare fiber which is a weak waveguide, no absorption by molecular overtones was detected.

VI. CONCLUSION

Waveguide architectures for detecting molecular overtones are discussed and the figure of merit is defined as the power in

the evanescent tail over the total power carried by the guided mode. An optimized structure is proposed for probing amine (N-H) overtone in the near-infrared spectrum on most common waveguide architectures, tapered waveguides, and microfibers. The advantages and disadvantages of each structure are discussed in terms of FoM, fabrication considerations, practical applications, optical strength, evanescent fields and modal confinement. We show that a tapered ridge and a tapered fiber structures exhibit an increased evanescent field, thus allowing for a strong interaction with the molecular layer. We also report that squeezing a silica fiber can achieve a higher evanescent field compared to the bare fiber and demonstrate this experimentally. However, for practical applications, the ridge structure is favorable due to its robustness and inertia to environmental changes. The methodology and outcomes presented in this work can be followed by performing detection of molecules or gasses.

REFERENCES

[1] A. Karabchevsky and A. Kavokin, "Giant absorption of light by molecular vibrations on a chip," *Sci. Rep.*, vol. 6, 2016, Art. no. 21201.

[2] H. F. Taylor and A. Yariv, "Guided wave optics," *Proc. IEEE*, vol. 62, no. 8, pp. 1044–1060, Aug. 1974.

[3] E. Ash, C. Pitt, and M. Wilson, "Integrated optical circuits for telecommunications," *Nature*, vol. 261, pp. 377–381, 1976.

[4] K. Xie *et al.*, "Fiber guiding at the Dirac frequency beyond photonic bandgaps," *Light, Sci. Appl.*, vol. 4, no. 6, pp. 1–8, 2015.

[5] Z. Rappoport, *The Chemistry of Anilines*. New York, NY, USA: Wiley, 2007, vol. 169.

[6] J. Hu *et al.*, "Fabrication and testing of planar chalcogenide waveguide integrated microfluidic sensor," *Opt. Express*, vol. 15, no. 5, pp. 2307–2314, 2007.

[7] A. Nitkowski, L. Chen, and M. Lipson, "Cavity-enhanced on-chip absorption spectroscopy using microring resonators," *Opt. Express*, vol. 16, no. 16, pp. 11 930–11 936, 2008.

[8] G. Li, C. M. de Sterke, and S. Palomba, "Figure of merit for kerr nonlinear plasmonic waveguides," *Laser Photon. Rev.*, vol. 10, no. 4, pp. 639–646, 2016.

[9] R. Zia, M. D. Selker, P. B. Catrysse, and M. L. Brongersma, "Geometries and materials for subwavelength surface plasmon modes," *J. Opt. Sci. Amer. A*, vol. 21, no. 12, pp. 2442–2446, 2004.

[10] P. Berini, "Figures of merit for surface plasmon waveguides," *Opt. Express*, vol. 14, no. 26, pp. 13 030–13 042, 2006.

[11] R. Buckley and P. Berini, "Figures of merit for 2D surface plasmon waveguides and application to metal stripes," *Opt. Express*, vol. 15, no. 19, pp. 12 174–12 182, 2007.

[12] R. Oulton, G. Bartal, D. Pile, and X. Zhang, "Confinement and propagation characteristics of subwavelength plasmonic modes," *New J. Phys.*, vol. 10, no. 10, 2008, Art. no. 105018.

[13] Z. Han and S. I. Bozhevolnyi, "Radiation guiding with surface plasmon polaritons," *Rep. Progress Phys.*, vol. 76, no. 1, 2012, Art. no. 016402.

[14] K. Okamoto, *Fundamentals of Optical Waveguides*. New York, NY, USA: Academic, 2010.

[15] R. R. Syms and J. R. Cozens, *Optical Guided Waves and Devices*. New York, NY, USA: McGraw-Hill, 1992.

[16] J. C. Boggio *et al.*, "Dispersion engineered silicon nitride waveguides by geometrical and refractive-index optimization," *J. Opt. Soc. Amer. B*, vol. 31, no. 11, pp. 2846–2857, 2014.

[17] R. A. Soref, J. Schmidtchen, and K. Petermann, "Large single-mode rib waveguides in GeSI-Si and Si-on-SiO$_2$," *IEEE J. Quantum Electron.*, vol. 27, no. 8, pp. 1971–1974, Aug. 1991.

[18] L. Vivien, S. Laval, B. Dumont, S. Lardenois, A. Koster, and E. Cassan, "Polarization-independent single-mode rib waveguides on silicon-on-insulator for telecommunication wavelengths," *Opt. Commun.*, vol. 210, no. 1, pp. 43–49, 2002.

[19] A. Durandet *et al.*, "Silica buried channel waveguides fabricated at low temperature using PECVD," *Electron. Lett.*, vol. 32, no. 4, pp. 326–327, 1996.

[20] M. Bazylenko, M. Gross, P. Allen, and P. Chu, "Fabrication of low-temperature PECVD channel waveguides with significantly improved loss in the 1.50-1.55-μm wavelength range," *IEEE Photon. Technol. Lett.*, vol. 7, no. 7, pp. 774–776, Jul. 1995.

[21] A. Roberts and M. Von Bibra, "Fabrication of buried channel waveguides in fused silica using focused MeV proton beam irradiation," *J. Lightw. Technol.*, vol. 14, no. 11, pp. 2554–2557, Nov. 1996.

[22] B. J. da Silva, R. P. de Melo, E. L. Falcão-Filho, and C. B. de Araújo, "Potassium source for ion-exchange glass waveguide fabrication," *Appl. Opt.*, vol. 36, no. 24, pp. 5949–5950, 1997.

[23] A. Miliou, H. Zhenguang, H. Cheng, R. Srivastava, and R. V. Ramaswamy, "Fiber-compatible K$^+$-NA$^+$ ion-exchanged channel waveguides: fabrication and characterization," *IEEE J. Quantum Electron.*, vol. 25, no. 8, pp. 1889–1897, Aug. 1989.

[24] R. V. Ramaswamy and R. Srivastava, "Ion-exchanged glass waveguides: A review," *J. Lightw. Technol.*, vol. 6, no. 6, pp. 984–1000, Jun. 1988.

[25] A. Karabchevsky, J. S. Wilkinson, and M. N. Zervas, "Transmittance and surface intensity in 3d composite plasmonic waveguides," *Opt. Express*, vol. 23, no. 11, pp. 14 407–14 423, 2015.

[26] A. Karabchevsky, S. Karabchevsky, and I. Abdulhalim, "Fast surface plasmon resonance imaging sensor using radon transform," *Sensors Actuators B, Chem.*, vol. 155, no. 1, pp. 361–365, 2011.

[27] A. Karabchevsky, S. Karabchevsky, and I. Abdulhalim, "Nanoprecision algorithm for surface plasmon resonance determination from images with low contrast for improved sensor resolution," *J. Nanophoton.*, vol. 5, no. 1, 2011, Art. no. 051 813.

[28] A. Karabchevsky, L. Tsapovsky, R. S. Marks, and I. Abdulhalim, "Study of immobilization procedure on silver nanolayers and detection of estrone with diverged beam surface plasmon resonance (SPR) imaging," *Biosensors*, vol. 3, no. 1, pp. 157–170, 2013.

[29] V. Lucarini, J. J. Saarinen, K.-E. Peiponen, and E. M. Vartiainen, *Kramers-Kronig Relations in Optical Materials Research*. New York, NY, USA: Springer, 2005, vol. 110.

[30] A. Karabchevsky, O. Krasnykov, M. Auslender, B. Hadad, A. Goldner, and I. Abdulhalim, "Theoretical and experimental investigation of enhanced transmission through periodic metal nanoslits for sensing in water environment," *Plasmonics*, vol. 4, no. 4, pp. 281–292, 2009.

[31] A. Karabchevsky *et al.*, "Metal grating on a substrate nanostructure for sensor applications," *Photon. Nanostruct.-Fundam. Appl.*, vol. 7, no. 4, pp. 170–175, 2009.

[32] A. Karabchevsky, M. Auslender, and I. Abdulhalim, "Dual-surface plasmon excitation with thin metallic nanoslits," *J. Nanophoton.*, vol. 5, no. 1, 2011, Art. no. 051 821.

[33] O. Krasnykov, A. Karabchevsky, A. Shalabney, M. Auslender, and I. Abdulhalim, "Sensor with increased sensitivity based on enhanced optical transmission in the infrared," *Opt. Commun.*, vol. 284, no. 5, pp. 1435–1438, 2011.

[34] A. Karabchevsky, C. Khare, B. Rauschenbach, and I. Abdulhalim, "Microspot sensing based on surface-enhanced fluorescence from nanosculptured thin films," *J. Nanophoton,*, vol. 6, no. 1, 2012, Art. no. 061 508.

[35] I. Abdulhalim *et al.*, "Surface-enhanced fluorescence from metal sculptured thin films with application to biosensing in water," *Appl. Phys. Lett.*, vol. 94, no. 6, 2009, Art. no. 063106.

[36] A. Karabchevsky, A. Mosayyebi, and A. V. Kavokin, "Tuning the chemiluminescence of a luminol flow using plasmonic nanoparticles," *Light, Sci. Appl.*, vol. 5, no. 11, 2016, Art. no. e16164.

[37] G. Brambilla, "Optical fibre nanowires and microwires: A review," *J. Opt.*, vol. 12, no. 4, 2010, Art. no. 043001.

Aviad Katiyi received the B.Sc. degree from the Lev Institute of Jerusalem, Jerusalem, Israel, in 2013. He is currently working toward the M.Sc. degree at the Ben-Gurion University of the Negev, Beer-Sheba, Israel. His current research interests include integrated photonics and molecular vibrations with guided-wave optics.

Alina Karabchevsky received the B.Sc., M.Sc., and Ph.D. degrees from the Ben-Gurion University of the Negev, Beer-Sheba, Israel, in 2005, 2008, and 2012, respectively. Since 2015, she has been with the Electrooptical Engineering Unit at Ben-Gurion University of the Negev and is a member of the Ilse Katz Institute for Nanoscale Science & Technology. She is the Head of the Light-on-a-Chip group. Her research activity is concentrated on waveguide-based platforms for emerging applications, such as sensing, quantum computing, optics telecommunication, and more.